Predisposition of the dark state of rhodopsin to functional changes in structure

ARTICLE *in* PROTEINS STRUCTURE FUNCTION AND BIOINFORMATICS · DECEMBER 2006

Impact Factor: 2.63 · DOI: 10.1002/prot.21158 · Source: PubMed

5 AUTHORS, INCLUDING:

Andrew J Rader
State Farm Insurance Co.
31 PUBLICATIONS **2,130** CITATIONS
SEE PROFILE

Judith Klein-Seetharaman
The University of Warwick
164 PUBLICATIONS **4,283** CITATIONS
SEE PROFILE

Ivet Bahar
University of Pittsburgh
291 PUBLICATIONS **12,024** CITATIONS
SEE PROFILE

PROTEINS: Structure, Function, and Bioinformatics 65:970–983 (2006)

Predisposition of the Dark State of Rhodopsin to Functional Changes in Structure

Basak Isin,[1] A. J. Rader,[1,2] Harpreet Kaur Dhiman,[3] Judith Klein-Seetharaman,[3] and Ivet Bahar[1]*

[1]*Department of Computational Biology, School of Medicine, University of Pittsburgh, Pittsburgh, Pennsylvania 15260*
[2]*Department of Physics, Indiana University-Purdue University Indianapolis, Indianapolis, Indiana 46202*
[3]*Department of Structural Biology, School of Medicine, University of Pittsburgh, Pittsburgh, Pennsylvania 15260*

ABSTRACT **As the only member of the family of G-protein-coupled receptors for which atomic coordinates are available, rhodopsin is widely studied for insight into the molecular mechanism of G-protein-coupled receptor activation. The currently available structures refer to the inactive, dark state, of rhodopsin, rather than the light-activated metarhodopsin II (Meta II) state. A model for the Meta II state is proposed here by analyzing elastic network normal modes in conjunction with experimental data. Key mechanical features and interactions broken/formed in the proposed model are found to be consistent with the experimental data. The model is further tested by using a set of Meta II fluorescence decay rates measured to empirically characterize the deactivation of rhodopsin mutants. The model is found to correctly predict 93% of the experimentally observed effects in 119 rhodopsin mutants for which the decay rates and misfolding data have been measured, including a systematic analysis of Cys→Ser replacements reported here. Based on the detailed comparison between model and experiments, a cooperative activation mechanism is deduced that couples retinal isomerization to concerted changes in conformation, facilitated by the intrinsic dynamics of rhodopsin. A global hinge site is identified near the retinal-binding pocket that ensures the efficient propagation of signals from the central transmembrane region to both cytoplasmic and extracellular ends. The predicted activation mechanism opens the transmembrane helices at the critical G-protein binding cytoplasmic domain. This model provides a detailed, mechanistic description of the activation process, extending experimental observations and yielding new insights for further tests. Proteins 2006;65:970–983.** © **2006 Wiley-Liss, Inc.**

Key words: G-protein-coupled receptors; collective dynamics; light activation; Gaussian network model; metarhodopsin II; elastic network; retinal isomerization

INTRODUCTION

Rhodopsin, the vertebrate dim light photoreceptor, is the prototypic member of the largest known superfamily of cell surface receptors, the G-protein-coupled receptors (GPCRs).[1] These receptors perform diverse functions including responses to light, odorant molecules, neurotransmitters, hormones, and a variety of other signals. The fact that 50–60% of all approved drugs target members of the GPCR family indicates the significant pharmacological importance of GPCRs.[2,3]

All GPCRs contain a bundle of seven transmembrane (TM) helices (H1–H7) originally observed by cryo-EM[4] and confirmed later by the X-ray crystal structure of rhodopsin in the inactive or dark state (Fig. 1).[5–9] This TM bundle encloses the chromophore, 11-*cis*-retinal, covalently bound to the ϵ-amino group of Lys296 on H7. 11-*cis*-retinal [Fig. 1(c)] is a derivative of vitamin A, consisting of a β-ionone ring (carbon atoms C1–C6), a polyene chain (C7–C15), and several methyl groups (C16–C20). The cytoplasmic (CP) domain of rhodopsin contains three interhelical loops, CL1–CL3, connecting the respective pairs of helices H1–H2, H3–H4, and H5–H6. In addition, there is a soluble helix H8, in the CP domain, which runs parallel to the plane of the membrane. The extracellular (EC) domain consists of the N-terminus and three interhelical loops (EC1–EC3) between TM helices H2–H3, H4–H5, and H6–H7, respectively. There is a β-sheet in the EC domain, located near the chromophore binding pocket. A portion of EC2 forms a β-strand that serves as a lid to the chromophore, running almost parallel to the polyene chain of the retinal and stabilized by a highly conserved disulfide bond between Cys110 and Cys187.[8]

The capture of a photon by rhodopsin induces the isomerization of 11-*cis*-retinal into all-*trans*-retinal. The structural perturbation in the retinal-binding pockets and TM helical bundle drives the passage through a series of photointermediates that ultimately lead to tertiary structure changes in the CP domain that are the

The Supplementary Material referred to in this article can be found at http://www.interscience.wiley.com/jpages/0887-3585/suppmat/

Grant sponsor: NIH-NLM; Grant number: 1R01LM007994; Grant sponsor: NSF ITR; Grant number: EIA0225636; Grant sponsor: NSF CAREER; Grant number: CC0449117.

*Correspondence to: Ivet Bahar, Department of Computational Biology, School of Medicine, University of Pittsburgh, Pittsburgh, PA 15260. E-mail: bahar@ccbb.pitt.edu

Received 7 March 2006; Revised 22 May 2006; Accepted 15 June 2006

Published online 28 September 2006 in Wiley InterScience (www.interscience.wiley.com). DOI: 10.1002/prot.21158

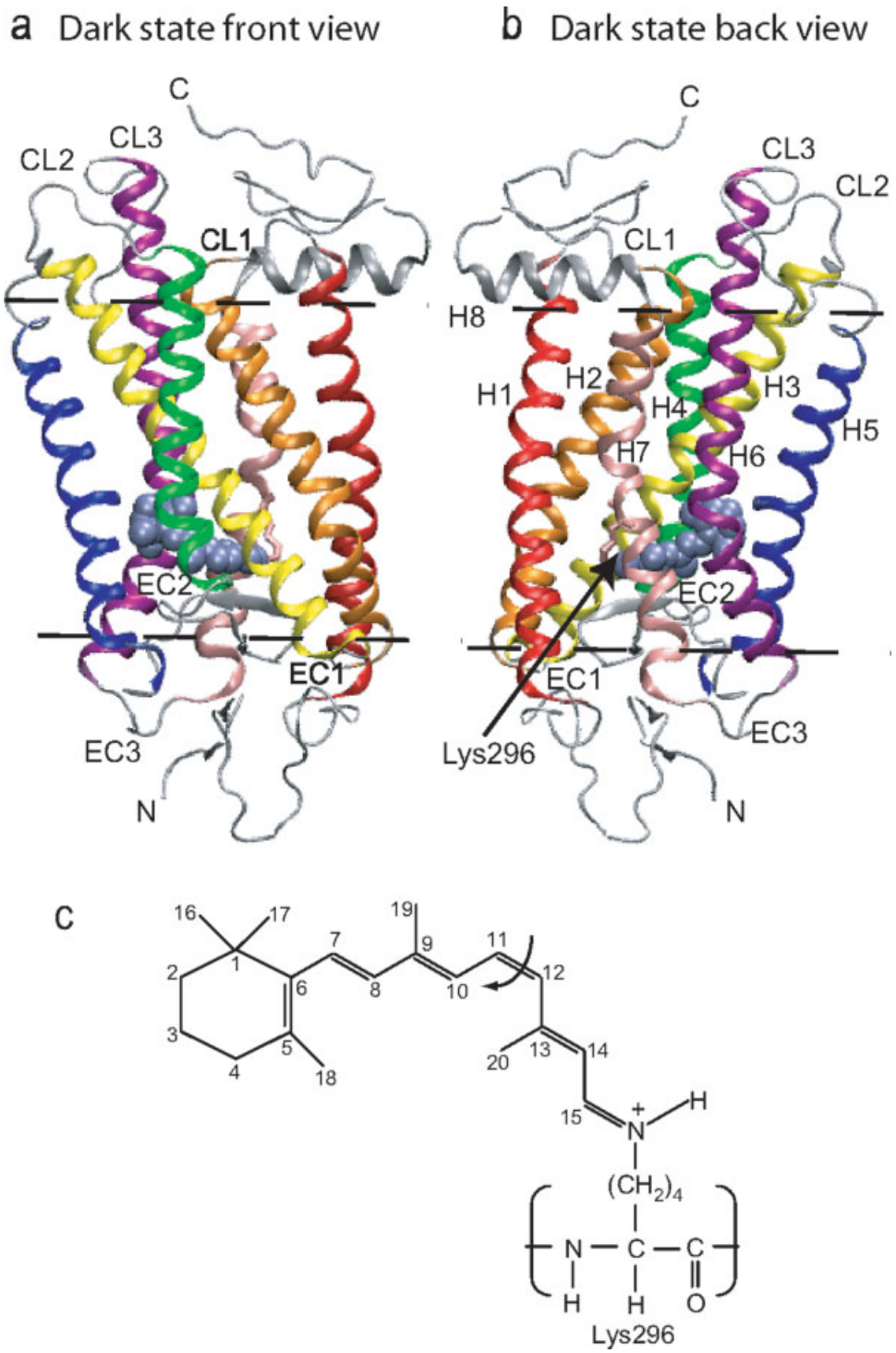

Fig. 1. Structure of rhodopsin in the dark state. (**a**) Front view. (**b**) Back view of the Protein Data Bank structure 1U19 deposited by Okada et al.[7] The structure contains seven transmembrane (TM) helices: Helix 1 (H1; residues 33–65), red; Helix 2 (H2; 70–101), orange; Helix3 (H3; residues 105–140), yellow; Helix 4 (H4; residues 149–173), green; Helix 5 (H5; residues 199–226), blue; Helix 6 (H6; residues 243–278), magenta; and Helix 7 (H7; residues 284–310), pink. The nonhelical portions and the CP helix 8 (H8) are in gray. 11-*cis*-retinal is shown in light-blue space-filling model. The dashed black lines show the approximate boundaries of the hydrophobic core of the membrane. The cytoplasmic and extracellular regions contain the respective loops CL1–CL3 and EC1–EC3. The side chain of Lys296 is displayed in the front and back view. (**c**) 11-*cis*-retinal and the protonated Schiff base linkage to Lys296. The arrow indicates the bond subject to *cis-trans* isomerization. This image was generated using VMD.[10]

hallmark of the active state of rhodopsin, metarhodopsin II (Meta II). The Meta II form binds the heterotrimeric G-protein, transducin, which is activated via exchange of GDP to GTP. Several other proteins interact with Meta II. In particular, rhodopsin kinase phosphorylates Meta II at the C-terminus, and arrestin binds to phosphorylated Meta II to terminate the signal.[11]

In the absence of a three-dimensional (3D) structure for the Meta II state, current knowledge on the activation mechanism of rhodopsin has been acquired from a range of biophysical and biochemical experiments with various degrees of detail. These include site-directed mutagenesis, photoactivity, NMR, and engineered disulfide bonds to rhodopsin and other GPCRs.[11–13] Such studies of the dark and light-adapted states of rhodopsin have suggested that the activation process is coupled to rigid body movements of the TM helices.[11] Accordingly, a conserved D(E)RY motif and other amino acids that interact with transducin are exposed via translations of H2, H3, H6, and H7, and rotation of H6. The term "rigid body" indicates that the helices maintain their secondary structures, although their relative positions and orientations in space undergo displacements.[12] The fluctuations are highest in the loops connecting the helices, as evidenced by the high flexibility of spin labels introduced in the CP loops, the formation of disulfide bonds between engineered cysteines located approximately 5–6 Å apart within the CP surface and the high B-factors observed in loop regions.[11,12] The movements of the helices during light-activation presumably involve the disruption of specific interhelical contacts and the release of the associated constraints. Despite the large body of literature on rhodopsin activation, the details of what drives these motions and the molecular interactions that underlie the experimental data on the Meta II state remain unknown. Epitomizing this lack of molecular understanding, the fluorescence decay rates observed for various rhodopsin mutants during Meta II deactivation are generally treated as "black box" values.[14] Our aim is to gain a better understanding of molecular mechanisms that drive the transition to the Meta II state by integrating experimental and computational results.

Because of the recent advances in efficient modeling and simulation of protein dynamics, there has been a flourish of computational analyses of the rhodopsin dark structure to suggest a structural model for the active state. The first molecular dynamics simulations of the photoisomerization process were performed by Rohrig et al.[15] and by Schulten and coworkers.[16] These simulations provided information on the early events of the opsin relaxation in response to light activation. More recent simulations spanning time scales up to 15 ns focused on the effects of lipids,[17,18] the time evolution of the chromophore isomerization accompanying the transition to the lumirhodopsin,[19] and the coupling between retinal and larger conformational changes.[17] However, the rhodopsin to Meta II transition, occurring in milliseconds, remains beyond the reach of molecular dynamics simulations that are usually confined to timescales on the order of tens of nanoseconds. Starting from a bathorhodopsin model,[20] structural models have been proposed for later photointermediates, including lumirhodopsin, Meta I, and Meta II by swinging the C- and N-terminal ends of H3 and rotating H6.[21] In other studies, distance constraints derived from NMR, EPR spectroscopy and/or disulfide bond formation experiments have been used to model the Meta II structure.[22,23] In another approach, results from energy calculations for the TM region and experimental data have been iteratively combined to generate a model for Meta II,[24] assuming the non-TM fragments to retain similar conformations in the dark and the light activated states. However, it is known from a large number of experiments that these regions, in particular the CP loops and the soluble H8, are highly mobile and their mobilities are important for activation.[12] Later, Marshall and coworkers built sets of low energy conformers for loops of rhodopsin both in the dark and the light activated states by using TM regions of their previous models as templates.[25]

The large scale motions required to fit experimental data suggest that other, faster computational methods are needed to explore the collective activation mechanism of rhodopsin. Elastic network models based on structural contact topology, and in particular the Gaussian Network Model (GNM)[26,27] built on the statistical mechanical theory of polymer networks,[28] provide efficient analytical solutions to macromolecular dynamics on a global (entire structure) scale. The conformational motions associated with low frequency slow modes predicted by the GNM and the anisotropic network model (ANM)[29] have been shown in several applications to provide insights about the mechanisms of cooperative motions of the *overall* molecule relevant to *function*.[30]* In particular, lowest mobility regions, or *minima* in the global modes, usually point to hinge or anchor sites, while *maxima* indicate the structural elements that can potentially serve as substrate recognition sites.[29–38] For example, the highly conserved shallow pockets that serve as receptor binding sites in influenza virus hemagglutinin A, or the antigen binding hypervariable loops of immunoglobulins, form maxima in the slowest mode shape, whereas linkers or interfacial regions between domains subject to anticorrelated motions form minima.[36] Complementary to the slow modes, the GNM/ANM high frequency (fast) modes provide information on *stability*. We have recently reported the use of GNM fast modes to identify the amino acids important for rhodopsin folding and stability using the dark state crystal structure as input. The results were strongly validated by experimental misfolding data: over 90% of the amino acids computationally predicted by GNM in conjunction with a thermal denaturation protocol to participate in the stability folding core were observed to cause misfolding when mutated.[34]

In this study, we present an in-depth analysis of the slow modes of motions predicted by the GNM/ANM, to characterize the global dynamics of rhodopsin in the dark state and identify mechanisms amenable to its acti-

*The atomic coordinates for the proposed ANM Meta II model are available upon request (bahar@pitt.edu).

vation. We combine these results to create an active, Meta II state model, which is refined and validated by comparisons to a variety of experimental data. We show that the opening of the helical bundle in the CP domain is favored by the intrinsic dynamic properties of rhodopsin, as a consequence of the particular topology of interresidue contacts in the dark state. Specifically, we identify a hinge site near the retinal binding pocket and show how this region coordinates the cooperative propagation of structural changes to the CP region. The opening of the helical bundle at the G-protein binding CP site is shown to be controlled by the concerted motion of the amino acids near the ligand binding pocket, providing a molecular explanation for structural changes observed upon formation of the active Meta II state, and a molecular interpretation of Meta II decay rates and disulfide bridge formation data.

METHODS

GNM and ANM

These two elastic network models have been introduced[26,27,29] and reviewed[30,37] in previous works. Here we describe the features relevant to the application to rhodopsin, only. The methodology essentially relies on the pseudoinversion and eigenvalues decomposition of a Kirchhoff matrix Γ of interresidue contacts (GNM) or Hessian matrix **H** (ANM) associated with the respective potentials of

$$V_{\mathrm{GNM}} = \frac{\gamma}{2}\sum_{i=1}\left[\left(\vec{R}_{ij} - \vec{R}^0_{ij}\right) \bullet \left(\vec{R}_{ij} - \vec{R}^0_{ij}\right)\right] h\left(R^{\mathrm{GNM}}_{\mathrm{cut}} - |\vec{R}^0_{ij}|\right) \tag{1}$$

and

$$V_{\mathrm{ANM}} = \frac{\gamma}{2}\sum_{i=1}\left(|\vec{R}_{ij}| - |\vec{R}^0_{ij}|\right)^2 h\left(R^{\mathrm{ANM}}_{\mathrm{cut}} - |\vec{R}^0_{ij}|\right) \tag{2}$$

where $\vec{R}^0_{ij}$ and $\vec{R}_{ij}$ denote the original and instantaneous distance vectors between residues i and j, represented by their C^{α}-atom positions, $h(x)$ is the Heaviside function equal to 1 if x is positive, and zero otherwise, and $R^{\mathrm{GNM}}_{\mathrm{cut}}$ and $R^{\mathrm{ANM}}_{\mathrm{cut}}$ are the cutoff distances for interresidue interactions, adopted here to be 10 and 15 Å, respectively, consistent with our previous work.[34,36] The mean-square fluctuations of residues and the cross-correlations between residues fluctuations are directly found from Γ^{-1} (or $\mathbf{H}^{-1}$). Of interest is to extract the contribution of the most cooperative fluctuations (mode $k = 1$) to equilibrium correlations, which is given in terms of the eigenvectors u_k and eigenvalues λ_k of Γ (or **H**) as

$$[\Delta\mathbf{R}_i \bullet \Delta\mathbf{R}_j]_k = (3k_BT/\gamma)\left[{\lambda_k}^{-1}\mathbf{u}_k{\mathbf{u}_k}^T\right]_{ij} \tag{3}$$

here k_B is the Boltzmann constant, T is the absolute temperature, γ is the uniform force constant usually of the order of 1 kcal/mol Å^2, found by requiring the sum of $\langle(\Delta\mathbf{R}i)^2\rangle$ over all residues ($1 \leq i \leq N$) to match the sum of the experimental B-factors. γ does not affect the residue distribution of motions in different modes, but uniformly rescales their absolute sizes. The kth eigenvector reflects the *shape* of the kth mode as a function of residue index (i.e., residue mobilities contributed by mode k), and the kth eigenvalue scales with the frequency of mode k.

Both GNM and ANM yield the equilibrium fluctuation dynamics of globular proteins around the native state. Low frequency modes predicted by the GNM/ANM permit us to identify global conformational changes relevant to function along with the critical sites controlling these changes. The peaks in the high frequency modes, on the other hand, point to key tertiary contacts that stabilize the overall fold.

Structures in the Dark State

The GNM and ANM were applied to two dark state crystal structures of rhodopsin deposited in the Protein Data Bank,[39] 1L9H[6] and 1U19A,[7] with 2.6 and 2.2 Å resolutions, respectively. Essentially identical slowest modes were found for these structures, consistent with the well-known robustness of such cooperative modes. Precisely, the first (slowest) GNM modes evaluated for 1L9H and 1U19a are verified to be almost indistinguishable, and equivalent to the linear combination of the first two modes (respective eigenvalues 0.29 and 0.32) computed by ANM for 1UL9A. The correlation cosine between the square displacements induced by GNM and ANM equivalent modes is 0.837. This mode was also verified to be the first (slowest) mode of motion for 1L9Ha. Based on these results, we concluded that this is the most robust mechanism of motion, and we reported the results based on this mode, referred to as the "global mode." The succeeding (lowest frequency) mode of motion was observed to give rise to a bending in the overall structure, which would be strongly hindered by the presence of surrounding lipid molecules, if the latter were explicitly included in the model. A drop-off has been observed in inverse eigenvalue in the case of higher modes, which justifies their omission from further analysis.

Generation and Refinement of ANM Structures

We generated two sets of fluctuating conformations, referred to as "positive" or "negative" deformations. These conformations are represented by the 3N-dimensional arrays of instantaneous position vectors $\{\mathbf{R}^+(s)\}$ and $\{\mathbf{R}^-(s)\}$ generated by a scaling the deformation induced by the global mode by the parameter s.[40] To determine which of these fluctuating conformations is more stable, and to correct for possible unrealistic distortions in bond lengths and bond angles, both sets of conformations were subjected to a short energy minimization scheme using MOE (Molecular Operating Environment) package, version 2001.01 (Chemical Computing Group, Montreal), with the Amber94 force field.[41] $\{\mathbf{R}^+(s)\}$ was observed to reach a substantially lower energy state compared to the $\{\mathbf{R}^-(s)\}$ (while both of them were higher than the energy minimized form of the dark state structure, as required), and the time elapsed to attain the equilibrated $\{\mathbf{R}^+(s)\}$ state was significantly shorter. $\{\mathbf{R}^+(s)\}$ was accordingly adopted as the Meta II model, using scaling factor, $s = 3$.

It is important to remember that this scaling factor is arbitrary. The motions predicted by our model provide a qualitative understanding of motions during activation; it does not allow predicting their absolute scales. However, the relative displacements found by the GNM/ANM are consistent with available experimental data (see Results and Discussion).

Metarhodopsin II Fluorescence Decay Measurements

Stability of the light-activated state can be quantified by measurement of the decay rate of Meta II, assuming that the destabilization of the equilibrium state will induce faster decays. To investigate position-specific contributions to Meta II stability, we collected the effects of 228 site-directed amino acid replacements in rhodopsin on the rates of Meta II decay from a survey of published and our own experiments. Ninety-seven of these corresponded to unique positions in the rhodopsin sequence. In all cases, Meta II decay was determined using the fluorescence assay developed by Farrens and Khorana.[14] Each mutant was measured using wild-type as a control. To compare different studies, we divided the mutant decay rates by the corresponding wild-type decay rates for a given set of experiments. A mutation was considered to have an effect on Meta II stability if the rates of decay were either enhanced or decreased by at least 20% with respect to the WT value. If a residue was predicted to be important (by GNM/ANM), but a Meta II decay rate had not been measured, we used data from misfolding experiments when available, since mutants that are not stable in the dark are not expected to be stable in the light either. When there were multiple experiments including different mutation backgrounds and different substitutions on the positions in question, we adopted the data supported by the larger majority of experiments. For eight residues, the experimental results were contradictory; therefore, we did not include those in our analysis (see Supplementary Table S3). In addition, we ignored the effects observed by drastic mutations, such as Gly to Glu, which would be expected to affect stability irrespective of a role in activation or stability. Thus, we generated a nonredundant dataset containing data on Meta II decay or dark state stability for 119 unique residues.

RESULTS AND DISCUSSION

A Hinge Region That Closely Interacts With the β-Ionone Ring of the Chromophore Coordinates the Collective Dynamics of the Protein

The global mode profile, that is, the residue displacements $[\Delta \mathbf{R}_i]_1$ in the most cooperative mode of motion, predicted for rhodopsin in the dark state are presented as a function of residue index i in Figure 2(a). The profile shows which regions move in the positive and negative directions along the principal axis of deformation induced by GNM mode 1, thus revealing which pairs of structural elements are subject to correlated and anticorrelated fluctuations. Also crossover residues between anticorrelated regions are found from the intersection with zero line (dashed). Panel (b) in Figure 2 displays the corresponding normalized square amplitudes $[(\Delta R_i)^2]_1$, also known as the *mode shape*, obtained with GNM (blue) and ANM (black), and panel (c) compares the theoretically predicted (red, GNM; blue, ANM) B-factors, $B_i = (8\pi^2/3)<(\Delta R_i)^2>$, and their experimental (X-ray crystallographic; black) counterparts. Note that the relative displacements of the structural elements are more distinctive upon examination of the global mode [panel (b)], as opposed to the B-factors that contain the contributions from a multitude of modes [panel (c)]. Panel (d) maps the panel (b) onto a color-coded ribbon diagram. The most constrained regions (minima in the global mode) are shown in blue, and maxima in orange.

The minima in the GNM/ANM global mode shapes usually point to residues implicated in mechanical roles relevant to biological function. Seven minima (Table I, column 1) are identified here by the GNM, the centers of which are labeled in Figure 2(b). Mapping these residues onto the ribbon diagram [Fig. 2(d)] reveals that they all lie in the middle of the TM helices, about halfway between the EC and CP regions, thus dividing the protein into two halves that experience anticorrelated motions. We note that Gly121, Glu122, Leu125, and Phe212 among these residues directly interact with the β-ionone ring of the chromophore in the dark state. The rest of the chromophore binding pocket lies immediately below the hinge region. This suggests that the isomerization of 11-*cis*-retinal into all-*trans* form during activation (see chromophore binding site analysis, below) is a cooperative process that can engage the entire TM helices by interacting with the global hinge region. The hinge residues are poised to transmit the conformational changes that trigger the new, activated conformation from the retinal-binding pocket to the CP and EC ends of the molecule.

Largest amplitude motions are predicted for the loop regions. The CP loops tend to have larger mobilities than the EC loops [Fig. 2(b)]. Interestingly, the loop EC2 is much less mobile than the shorter CP loops CP2 and CP3. This suggests that there is a possibly larger conformational motion upon retinal isomerization on the CP side than the EC side.

Opening of the Helical Bundle by a Cooperative Torsion of the TM Helical Bundle

The GNM analysis also provides information on the *size* of collective motions. Information on the *directions* of motions, on the other hand, is obtained by ANM analysis (see Methods). The global mode shape obtained by the ANM, shown by a black curve in Figure 2(b), matches well its GNM counterpart. An additional minimum appears in the mode shape by ANM in loop EC3 containing the residues Pro180 and Cys187 which constrain the EC entrance to the chromophore binding pocket.

The structure deformed according to ANM [and refined by energy minimization (see Methods)] is the

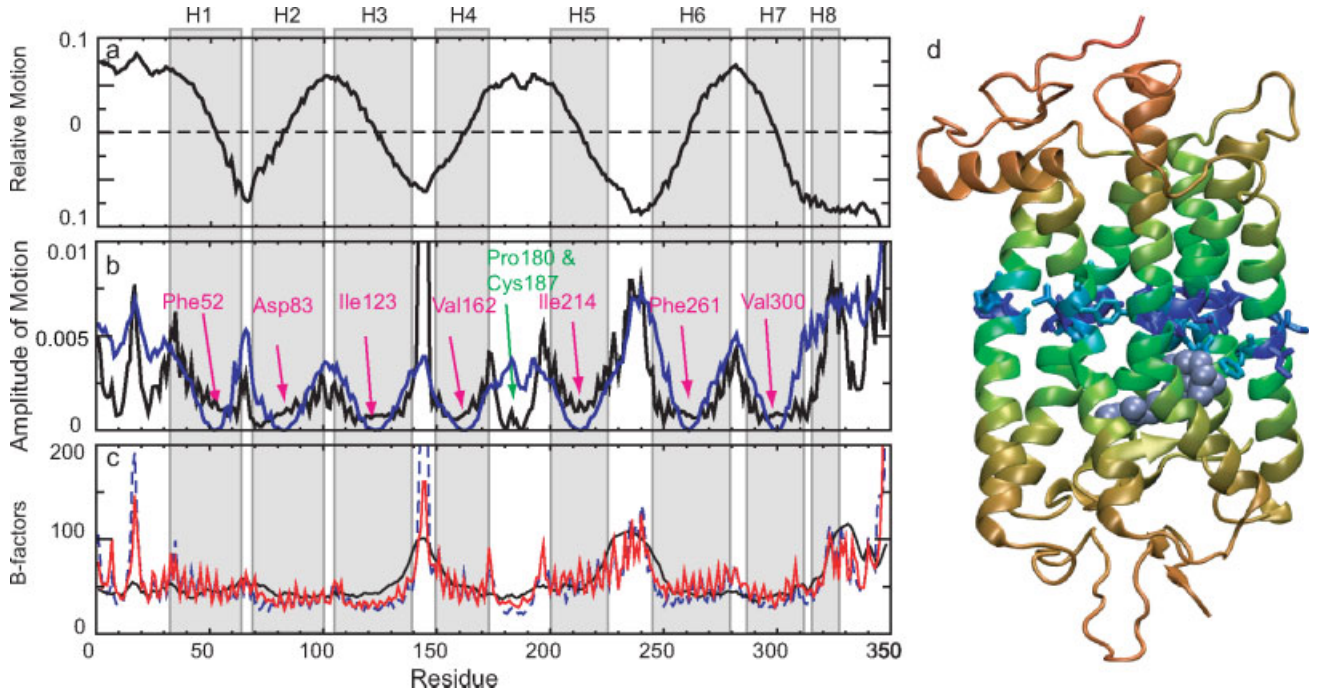

Fig. 2. Predicted mobilities and motions by GNM and ANM. (**a**) The global mode profile calculated with GNM, indicating the relative motions of different regions of the proteins along the principal (normal) mode coordinate. The curve is directly given by the elements of the eigenvector associated with the slowest nonzero mode. Positive and negative regions delineate structural blocks subject to concerted motions. The zero-crossing points serve as hinges between anticorrelated regions. The locations of the helices (H1–H8) are indicated on the upper abscissa and distinguished by gray bands. (**b**) The distribution of square displacements of residues predicted by the GNM (blue) and ANM (black). The non-TM regions exhibit higher mobilities in general, especially CL2 (between H3 and H4) and CL3 (between H5 and H6). Residues acting as hinge centers (minima near the middle of each TM helix) are labeled. The ANM yields two additional minima: Pro180 and Cys187 near the EC entrance to the chromophore binding pocket. (**c**) Experimental (black) and predicted thermal B-factors from GNM (red) and ANM (dashed blue). (**d**) Ribbon diagram of rhodopsin color-coded according to the relative motions in (b) in the order of increasing mobility blue (lowest mobility), cyan, green, yellow, orange, red (highest mobility). The side chains are shown for the seven GNM hinges labeled in (b) and 11-*cis*-retinal is shown in light blue space-filling representation. The hinge site divides the protein into two anticorrelated regions: one on the CP side and the other containing the chromophore binding pocket on the extracelluar side. This image was generated using VMD.[10]

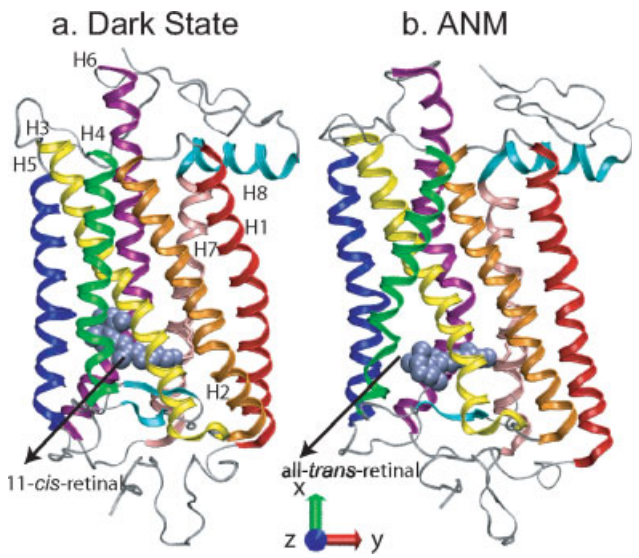

Fig. 3. Comparison of the dark state structure (**a**) and ANM-predicted structure proposed for the Meta II form (**b**). The colors of the TM helices are consistent with Figure 1(a). The dark and ANM structures contain the chromophore in the 11-*cis* retinal, and all-*trans* isomeric forms, respectively. This image was generated using VMD.[10]

predicted Meta II state. The differences between the dark state and the ANM state are shown in Figures 3 and 4. Figure 3 shows a side view of the two structures, and Figure 4 presents a series [panels (a–e)] of cross-sectional slices separated by 10 Å along the cylindrical axis, starting from the CP region [panel (a)]. For reference, the residue numbers on H6 that are part of a given slice are also given. The comparison between the two structures reveals that there is an overall torsion or twisting of the molecule involving all of the TM helices. This is consistent with the identification of global hinges spread across all the TM helices [Fig. 2(b)]. The CP ends of all helices undergo a counterclockwise rotation in the ANM-predicted state, relative to their positions in dark state, when viewed from the CP end [panels (a) and (b)], while the opposite (EC) end of the helices display a clockwise rotation [panels (d) and (e)]. The retinal binding pocket is located in panel (d). Accompanying this torsional motion is an overall expansion in the cross-sectional areas at two ends of the TM region, while the central region remains almost unchanged.

There are a number of additional features predicted by ANM that merit a more detailed examination. First, H6

TABLE I. Residues Indicated by GNM/ANM to Play a Critical Role in Functional Dynamics

	Amino acids affected by retinal isomerization			
Global hinge sites (minima in global mode shapes)	Stabilizing retinal in the dark state	Clashing with *trans* retinal in the dark state	Stabilizing all-*trans* retinal in the Meta II state	Peaks in high frequency modes[34]
Gly51, Phe52, *Pro53* (H1); Ala82, *Asp83*, Leu84 (H2); *Gly121*, *Glu122, Ile123*, Ala124, *Leu125* (H3); Trp161, Val162, Met163, *Ala164* (H4); Phe212, Ile213, Ile214 (H5); Ala260, *Phe261* (H6); Ala299, Val300, Tyr301 (H7)	*Glu113* (H3); *Ala117* (H3); *Thr118* (H3); *Glu122* (H3); *Met207* (H5); *His211* (H5); Phe212 (H5); *Phe261* (H6); *Trp265* (H6); Tyr268 (H6); Ala269 (H6)	*Thr118* (H3); *Cys167* (H4); Ala168 (H4); *Pro171* (H4); *Tyr178* (H5); *Gly188* (β4); Ile189 (β4); *Phe203* (H6)	*Thr118* (H3); *Cys167* (H4); Ala168 (H4); Ala169 (H4); *Pro171* (H4); *Leu172* (H4); *Tyr178* (β3); *Ser186* (β4); *Cys187* (β4); Ile189 (β4); *Phe203* (H5); *Trp265* (H6); Tyr268 (H6); *Ala295* (H7)	*Pro23 Asp83*; Met86 *Val87*; Phe91 *Thr94 Ser98*; Gly101 *Tyr102*; *Phe103 Cys110*; *Glu113 Gly114*; Phe115 *Ala117*; Gly120 Ala124; *Tyr178 Pro180*; *Glu181 Met183*; *Gln184* Cys185; *Ser186 Cys187*; *Ala292* Ala299

The associated secondary structural elements are given in parentheses; residues in italic are confirmed by Meta II decay experiments to play a critical role.

(magenta) rotates and extends into the cytoplasm as can be viewed in Figures 3(b) and 4(a). Second, H3 (yellow) seems to assume a pivotal, central position [Fig. 4(c)]. In the ANM predicted structure, H3 is more exposed (than in the dark state) to the cytoplasm. In the dark state, it closely interacts with H4 (green) near the CP interface while simultaneously interacting with H2 (orange) near the EC interface [Fig. 3(a)]. Facilitating the exposure of its CP end to the cytoplasm is the motion of H4 away from H3, stretching the loop CL2, and creating a cavity that provides access to amino acids in H3 and CL2. This outward radial motion of the CP end of H4 is compensated by a motion in the opposite direction at its EC end, moving it closer to the retinal (see chromophore binding pocket analysis, below). Other helices also readjust their positions, resulting in an overall opening of the helical bundle at the CP side. H1 (red) forms a kink at Gly51–Pro53, resulting in a bending at the CP part of H1 away from the bundle. Similarly, H7 bends at Ala299 and also rotates around this residue. The soluble and highly mobile helix H8 (cyan) rotates within the plane perpendicular to the TM helices, as can be seen in Figure 4(a). At the EC side, the torsions of helices also result in an opening of the helical bundle, but of a smaller magnitude than at the CP side. The innermost pair of β strands, β3 and β4, is highly constrained and remains almost fixed in space [Fig. 4(e)].

Chromophore Binding Pocket Analysis: Dark State Structure Cannot Accommodate all-*Trans*-Retinal

The reconfiguration of 11-*cis* retinal in the dark state to all-*trans* form in the ANM structure can be seen in Figure 3(a,b), respectively. To understand more closely how all-*trans*-retinal triggers the destabilization of the dark state structure upon isomerization, the dihedral angle or the bond between carbon atoms C11 and C12 [see the arrow in Fig. 1(c)] was rotated by 180° within the context of the dark state structure, followed by a short energy minimization protocol that retains the retinal in the *trans* form. Figure 5(a,b) show the neighborhood of the chromophore, in the *cis* and *trans* forms of retinal, respectively, when that the dark state structure remains unchanged. Opsin heavy atoms within 4.5 Å of the retinal are displayed in each case. Because all-*trans*-retinal is more extended than 11-*cis*-retinal, isomerization leads to steric clashes with the opsin, unless relieved by suitable conformational rearrangements. The rhodopsin residues that show steric clashes with all-*trans*-retinal atoms are listed in Table I, column 3. Most of these clashes involve the β-ionone ring of the chromophore. The large number of steric clashes confirms previous notions[16,20] that a rigid dark state structure cannot accommodate all-*trans*-retinal. Therefore, the molecule must adopt a new conformation with a larger chromophore binding pocket that can accommodate the all-*trans* isomer of retinal.

Photoisomerization Changes the Network of Interactions in the Chromophore Binding Pocket

The chromophore binding pockets in the dark state and in the ANM Meta II structure are shown in Figure 5(a,c), respectively. Of the interactions between the opsin protein and the retinal, those involving the β-ionone ring are the most strongly affected by isomerization. This is due to the relocation of the β-ionone ring to a different environment upon isomerization and the rearrangement of the helices at the chromophore binding site to accommodate the new conformation of the retinal. In the dark state, the β-ionone ring is highly constrained by contacts

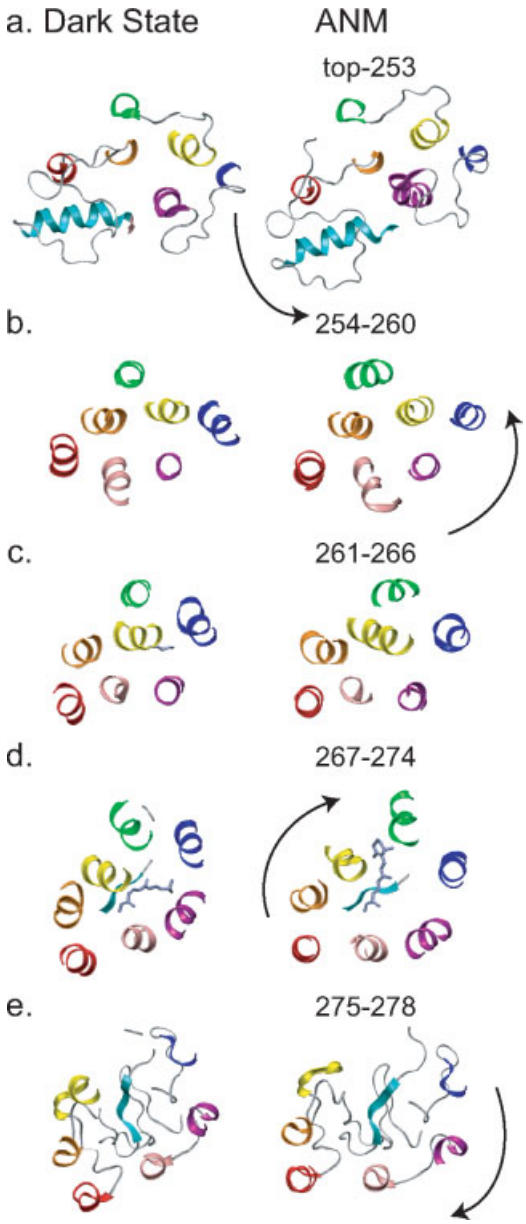

Fig. 4. Comparison of the two structures viewed from top. Cross-sectional views of slices of 10 Å, displayed for dark state structure (left column) and ANM-predicted Meta II structure (right column). The slice corresponding to the chromophore binding site is shown in (**d**). Note the counter-rotation of the CP and EC ends of the structure in the ANM structure, indicated by the arrows to guide the eye. Residue indices corresponding to H6 residues are given to indicate the position of the respective slices. This image was generated using VMD.[10]

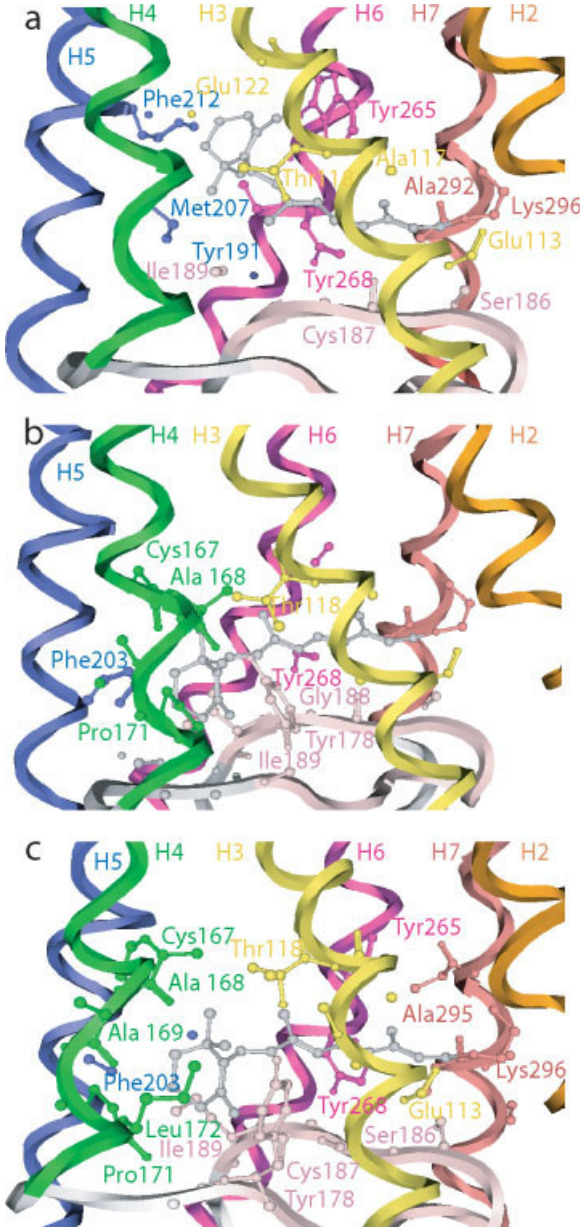

Fig. 5. Close neighborhood of the chromophore in the dark state before (**a**), and after (**b**) isomerization of the retinal to *trans*-form, and in the ANM predicted form (**c**). (a) The dark state structure contains retinal in the 11-*cis* form. Its β-ionone ring is stabilized by Glu122 at H3, Met207 at H5, His211 at H5, Phe212 at H5, Phe261 at H6, Trp265 at H6, Ala269 at H6. (b) There are steric clashes between all-*trans*-retinal and opsin residues in the chromophore binding pocket in the dark state structure of rhodopsin. All heavy atoms of opsin within 4.5 Å of all-*trans*-retinal are displayed. The residues that clashes with all-*trans*-retinal are Thr118, Cys167, Ala168, Pro171, Tyr178, Gly188, Ile189, and Phe203. (c) The ANM Meta II structure with all-*trans* retinal where all steric clashes are relieved. The polyene carbons C9–C15, C19, and C20 have common neighboring residues in both structures. These residues include Thr118 at H3, Tyr268 at H6, Cys187 and Gly188 at β4, Gly114, Ala117 and Glu113 at H3, Lys296 at H7, and Ile189 at β4. In addition to these common residues, Tyr178 and Cys181 at β3 interact with the polyene chain of the retinal at the ANM Meta II structure. Tyr178 runs parallel to the β-ionone ring of all-*trans*-retinal. This image was generated using VMD.[10]

made with H3, H5, and H6, [Fig. 5(a) and Table I column 2]. The ANM Meta II structure with all-*trans*-retinal, in contrast, identifies residues from H4, H3, and β-hairpin at the EC loop EL2 that stabilize the β-ionone ring [Fig. 5(c) and Table I column 4]. The most pronounced new constraints imposed on the ring are by the β-hairpin, in particular Tyr178 and Ile189, and by H4 such as Cys167, Ala168, Ala169, Pro171, and Leu172.

Comparison with Structural Changes Experimentally Observed Upon Activation of Rhodopsin and Other GPCRs

The current model for the mechanism of activation by light in rhodopsin and by ligands in GPCRs in general is essentially composed of two aspects: (1) induced conformational changes, which simultaneously (2) release structural constraints. Much work has focused on identification of both the nature of the conformational changes and the key structural constraints ("*microdomains*") shared by the GPCR family.[42–59] These include (i) an ionic interaction region between the charges of ligand and receptor, corresponding to retinal Schiff base and the Glu113 counter-ion in rhodopsin,[46,59] (ii) a D(E)RY motif at the CP end of H3 and the $X_1BBX_2X_3B$ motif at the CP end of H6 (B, basic; X, nonbasic),[42–44,47–52,58] (iii) a Asn–Asp pair at H1 and H2, respectively, and a NPXXY motif in H7,[6] and (iv) an aromatic cluster surrounding the ligand binding pockets.[54–57] In the following, we will compare the experimentally observed changes to those predicted by the ANM.

Changes observed in retinal–rhodopsin contacts upon activation

Photoaffinity labeling and cross-linking experiments indicate that retinal isomerization is accompanied by a change in the neighboring amino acids, in particular those contributing to the aromatic cluster (microdomain iv) that coordinate the chromophore. The β-ionone ring of 11-*cis*-retinal can be cross-linked to Trp265 on H6 in the dark state, but not after light-activation.[55] Instead, Ala169 from H4, a residue located >10 Å away from the ionone ring in the dark state,[8] forms a cross-link with retinal in the light, but not in the dark[54] These observations are in good agreement with our findings, illustrated in Figure 5. In the dark state, Trp265 is located immediately adjacent to the β-ionone ring toward the CP side, while Ala169 does not interact with the retinal.[8] In contrast, in the predicted active structure with all-*trans*-retinal, Ala169 interacts closely with the atoms of β-ionone ring while Trp265 does not.

Experimental evidence for the opening of the CP side of TM helical bundle

Extensive Cys scanning mutagenesis along the CP surface of rhodopsin in combination with site-directed spin labeling followed by EPR analysis of mobility, accessibility and spin–spin interactions, sulfhydryl reactivity, and disulfide cross-linking rates measurements have been performed to deduce the molecular nature of the conformational changes accompanying activation.[11,13,60–66] In particular, the mobility of spin-labeled side chains at the buried surfaces of H1, H2, H3, H6, and H7 are found to increase upon isomerization.[11] This indicates reduced packing in the core of the protein. Furthermore, several sets of pairs of Cys suggest that there is an increase in the relative distances between the CP ends of helices, especially between H3 and H6.[11] Six of these disulfide bridges (138–251, 139–247, 139–248, 139–249, 139–250, 139–251), connecting H3 and H6 close to their CP end, prevented the light activation of rhodopsin.[65,67] This indicates that the relative positions of H3 and H6 change during activation. Figure 6(a) illustrates the relative positions of these disulfide-bridge forming sites in the

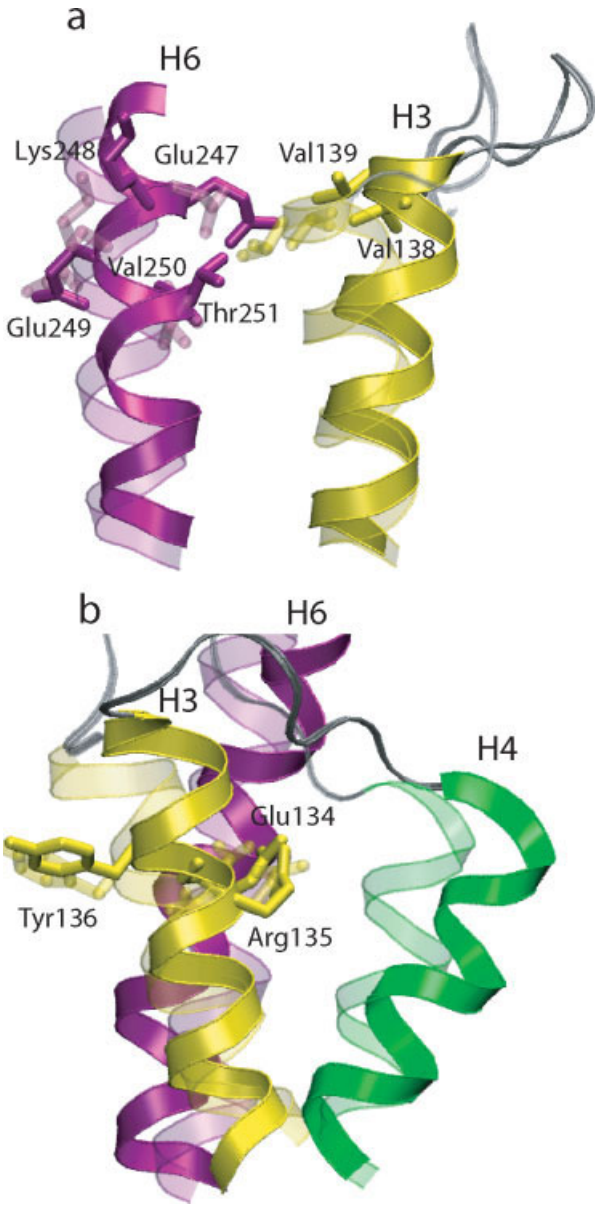

Fig. 6. Repositioning of CP ends of H3, H4, and H6 in the ANM Meta II (opaque) and dark state (transparent) structures. (**a**) Relative movements of H3 and H6. The residues shown as sticks are detected by disulfide cross-linking studies to inhibit the light activation of rhodopsin when mutated to Cys.[65] (**b**) Position of the ERY motif in the dark state and the ANM Meta II structures, showing how the ERY motif becomes more surface-exposed in the proposed Meta II form due to the local rearrangements of helices in its close neighborhood, including in particular the displacement of H4 away from H3 and H6. The surface accessibility of the ERY motif residues Glu134 and Arg135 increases from 23.6 to 29.7 $Å^2$ and from 14.2 to 25.5 $Å^2$, respectively, while Tyr136 being already solvent-exposed does not exhibit a significant change in solvent accessibility. This image was generated using VMD.[10]

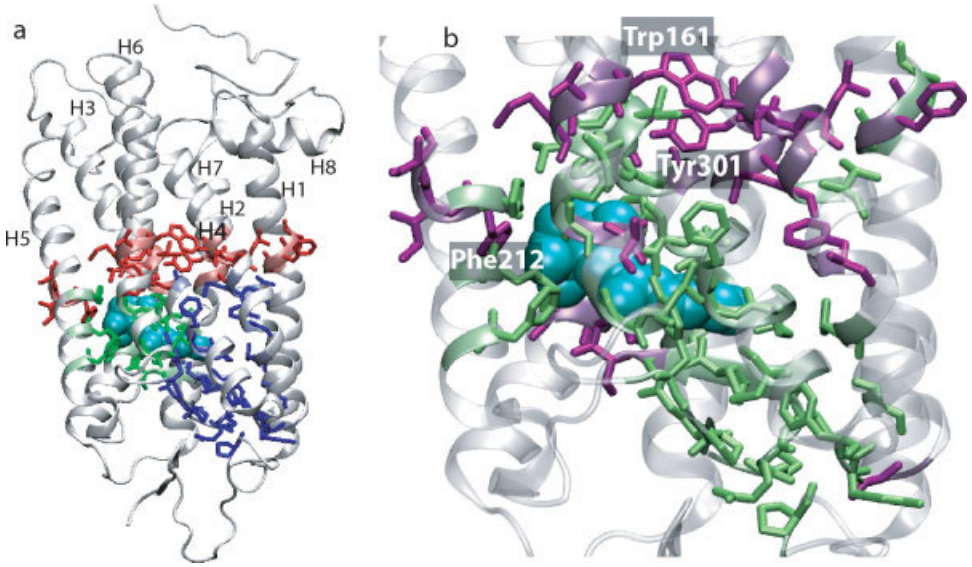

Fig. 7. (**a**) Residues identified by GNM/ANM to play a key role, colored by their different roles in the global mechanics and/or function; global hinge sites in red, amino acids affected by retinal isomerization in blue, and peaks in high frequency modes in green (**b**) a closer look of the same subset of residues identified by GNM to play a key role. Those confirmed by Meta II and folding experiments to play a critical role are colored green, and the rest, purple. Both structures refer to the dark state conformation with 11-*cis* retinal shown in space-filled model colored cyan. This image was generated using VMD.[10]

dark state (transparent) and in the Meta II ANM structure (opaque). A smaller displacement in the CP ends of H1 and H2 away from H7 has also been detected experimentally (microdomain iii), consistent with the ANM-predicted increase in surface accessibility at the CP region. It is noteworthy to observe that the surface accessibility of the G-protein contact site near the ERY motif (microdomain ii) increases upon transition from the dark state structure to the ANM-predicted deformed structure. The surface accessibility of the ERY motif residues Glu134 and Arg135 in particular increases from 23.6 to 29.7 $Å^2$ and from 14.2 to 25.5 $Å^2$, respectively, while Tyr136 being already solvent-exposed does not exhibit a significant change in solvent accessibility. Figure 6(b) shows the ERY motif both in the dark state (transparent) and ANM-predicted deformed state (opaque) and change in the relative positions of the CP ends H3, H4, and H6.

The above comparison with experimental observations support the ANM predicted structural changes, including those affecting the microdomain constraints. In the next section, we will discuss the new insights gained by GNM/ANM analysis on the activation mechanism. This includes an explanation of the effects of mutations on Meta II stability, how refinements using atomistic details impact the model for rhodopsin activation, and a mechanistic explanation of the observed conformational changes and their implications for G protein binding and activation.

Analysis of Meta II Decay Rates of Rhodopsin Mutants in Light of Key Residues Identified by GNM/ANM

Empirical characterization of rhodopsin mutants typically includes investigation of Meta II stability by way of quantifying Meta II decay rates.[14] While a useful measure to estimate the role of a given amino acid in structure and function, Meta II decay rates have been mostly phenomenological, providing little insight into the mechanisms by which stability is altered. Here, we provide such mechanistic insight using GNM/ANM results.

We presently identified three groups of residues of interest, listed in Table I: (i) those participating in the global hinge region, (ii) the amino acids directly affected by retinal isomerization (Figs. 4 and 5), and (iii) the residues emerging as peaks in GNM/ANM fast modes, that is, distinguished in the high frequency modes. The former two groups are identified in the present study, and the latter in our previous work.[34] These three groups of residues are colored red, blue, and green, respectively, in Figure 7(a). Note that some of the residues are included in more than one group, overall summing to 61 residues implicated in functional interactions/dynamics (Table I).

For comparative purposes, we compiled a comprehensive list of Meta II decay rates in mutants of rhodopsin from the literature (see Supplementary Table S1), and conducted further experiments (see below and Table II). In the absence of Meta II decay rates, we resorted to data from misfolding experiments when available. This led to a dataset of 127 distinctive residues with known Meta II or dark state stability. If the ratio μ of the mutant decay rate to WT decay rate ($\mu = r_m/r_{wt}$) lies within the range $0.8 \leq \mu \leq 1.2$, the mutation is assumed to be inconsequential; otherwise, the mutation is assumed to affect stability/function. Based on this criterion, 45 amino acid replacements were found to have an effect on Meta II stability and/or misfolding, while 74 were inconsequential; 8 of the 127 residues had contradictory results and have not been included in our comparative analysis.

TABLE II. Rhodopsin Mutants and Their Meta II Half-Life

Mutant	Meta II half-life (min)	Ratio between Meta II half-lives of mutants and the WT
WT	15.9	1.00
C140S	15.1	0.95
C167S	25.5	1.60
C222S	12.8	0.81
C264S	18.9	1.19

Our objective was to see if the 61 residues inferred by GNM/ANM to play a critical role (Table I) were also observed by experiments to impair decay or folding properties (true positives, TPs), while the other residues (not predicted by GNM/ANM to play a key role) were confirmed to be inconsequential (true negatives, TNs). The comparison between theory and experiments yielded 38 TPs [written in italic in Table I, colored green in Fig. 7(b)], 1 false positive, 73 TNs, and 7 false negatives. In 111 out of 119 experimentally examined cases, GNM/ANM was therefore able to correctly predict the experimental outcome. Thus, the GNM/ANM results can help explain 93%, of the experimental data on mutant's Meta II decay rates (and folding), correctly. We note that experimental data are not (yet) available for 21 residues [colored purple in Fig. 6(b)], and ambiguous for one residue, indicated to be important by GNM/ANM analysis. The observed validation with available experimental data, whenever available, strongly supports the use of GNM/ANM predictions for guiding future experiments. It remains to be seen if these 21 residues play an important role for Meta II stability or folding properties. In particular, we note among them a few aromatic residues, Tyr301, Trp161, and Phe212, which appear to play a central role in stabilizing the global hinge region (Fig. 7b).

The accuracies of the above calculations are limited by the fact that the mutations reported in the literature vary in their severity. For example, replacement of a Cys by an Arg is more severe than replacement by a Ser, especially in a membrane environment. To provide further testing of the predictive value of GNM/ANM Meta II effect analysis, we generated a small dataset in which Cys residues at positions 140, 167, 222, and 264 were replaced with Ser one at a time and the Meta II decay rates were measured under identical conditions. Table II lists the results. The only significant effect was by the Cys167Ser substitution. The comparison of the dark and ANM structures provides a plausible explanation for this result. In the dark structure, Cys167 shows steric clashes with C1, C2, and C16 atoms of all-*trans*-retinal. This result validates our approach, since the increase in Cys167Ser Meta II stability cannot be explained by inspection of the dark state crystal structure. Instead, it can be well understood from the differences in the retinal binding pockets in the dark and in the ANM structures. For the other three cysteines investigated experimentally here, ANM/GNM correctly predicted that amino acid replacement at these sites does not have an effect on Meta II stability.

Refining the Current Model for Activation of Rhodopsin

The predicted Meta II model identifies several previously unknown details. For example, H4 emerges as a structural element playing an important role in transmitting the activation signal from the chromophore binding pocket to the cytoplasm. Triggered by steric clashes within the chromophore binding region, H4 undergoes significant rigid body reorientation with respect to the cylindrical axis, and this reorientation is reflected in large displacements at both the CP and EC ends. At the chromophore binding pocket the displacement of H4 is more than 4 Å, outward the helical bundle. In particular, the CP end of H4 moves away from the helical bundle resulting in an extension of CL2 between H3 and H4 and exposure of the ERY motif in H3 [constraint ii, above; Fig. 3(b) and (b)]. Thus, in contrast to the prevailing view of activation,[13] it is not simply the relative displacement of H3 and H6 with respect to each other that produces the critical conformational changes recognized by the G protein. Likewise, a decrease in the mobility of Thr70 and Tyr74 in H2, Arg147, and Phe148 in CL2 have been attributed to the movement of H2 toward H4.[11,64] The ANM analysis shows that H4 moves closer to H2.

The motion of H6 deduced from increases in the accessibility of Val250 and Thr251 at H6 upon activation[60] and the changes in distances of a range of spin labels on H6 with respect to Val139Cys in H3[65] were previously attributed to the movement of H6 away from the helical bundle so that it interacts less with helices such as H3 and H7. The GNM shows that four CP turns of H6 are extremely mobile and tend to extend toward the cytoplasm facilitated by a screw-like torsional rotation of H6.

Finally, conformational changes in the EC domain have not been investigated extensively by experiments previously. Our ANM results show that the opening of the helical bundle in the CP domain through torsional rotation in one direction is coupled to an opposite direction rotation in the EC side, which also induces an opening of the helical bundle at the EC end. This observation is in accord with findings that the disulfide bond at the EC-TM interface becomes accessible to reducing reagents upon light activation. The results seem to support the hypothesis that EC2 moves upon activation, releasing constraints imposed by its interactions with helices H4 and H5 that help lock the receptor in an inactive conformation in the dark.[68,69] Further quantitative testing the ANM predictions will require distance measurements between spin labels placed in the CP and EC domain simultaneously. Double electron–electron resonance experiments will allow such long-range distance measurements.

A Mechanistic Explanation for Experimentally Observed Conformational Changes in Rhodopsin and Implications for the Activation of G Proteins

The transmission of the signal of retinal isomerization to the CP domain, and induced opening of the helical bundle CP end to allow for G protein binding is ensured by a

global hinge site spatially located in the close neighborhood (and directly interacting with) the retinal-binding pocket [Fig. 2(b,d)]. This site divides rhodopsin into two coupled but anticorrelated regions: one on the G-protein binding, CP side and the other on the EC side surrounding the chromophore binding pocket. The global motion coordinated by the hinge region is essentially manifested by increasing mobility toward the CP portions of H3–H6. The interactions at the hinge site with the retinal, predominantly with its ionone ring, restrict H6. Isomerization of the retinal into the *trans* form releases these interactions, resulting in an extension of H6 toward the cytoplasm and rotation around its own axis [Figs. 3(b) and 4(a)]. On the other hand, *cis–trans* isomerization potentially entails steric clashes between H4 and the β-ionone ring, which are relieved by the repositioning of H4. Furthermore, while H5 stabilizes 11-*cis*-retinal dark state opsin interactions together with H3 and H6, it bends at its hinge and therefore interacts less with all-*trans* retinal in the activated state [Fig. 3(b)]. This combination of release of constraints or weakening of interactions, accompanied by the formation of new interactions is readily achieved by an overall torsional motion of the molecule driven by the first (global) collective mode. Thus, there is a clear cooperativity between the changes in the chromophore environment and the conformational changes in the CP domain upon light-activation, which can be explained by the intrinsic dynamic properties of rhodopsin in the dark state.

In summary, our results support the view that the dark state structure of rhodopsin is predisposed to undergoing the large scale structural changes that are experimentally observed to be triggered upon light-induced retinal isomerization. This predisposition is unambiguously revealed by the global vibrational or relaxational fluctuations naturally favored by the topology of interresidue contacts before light-activation.

It is a generally accepted notion that the opening of the helical bundle is the critical event for binding and activation of G protein, transducin, by (1) generating a cavity that provides sufficient space/volume for interaction and (2) exposing specific residues involved in direct recognition and binding.[13] Our model suggests that beyond these two general notions, we can now state that an overall torsional motion of the TM domain, that simultaneously induces the opening of the CP end of the TM bundle and the screwing motion of H6, underlie the conformational transitions that facilitate transducin binding leading to GDP/GTP exchange.

CONCLUSIONS

In the present study, we presented a robust model for the light-activated Meta II state of rhodopsin, the prototypical member of the GPCR family. We show that information for functional conformational changes as they occur upon formation of the activated structure of rhodopsin, Meta II, is encoded largely in its inactive dark state structure. The relevance of the modeling results to the conformational changes conducive to the Meta II state is validated by a large amount of experimental data. More important, the newly proposed Meta II state model reveals previously unknown molecular details. Only a subset of these newly identified motions has been studied experimentally so far, and the model therefore provides a useful framework for further experimental validation.

It appears that there are only a few specific contacts that restrict the structure in a "locked" dark state, while the overall molecule possesses the potential to undergo highly concerted fluctuations and efficiently transmit signals from the chromophore binding domain across the TM region to both CP and EC domains. The inference is that it is not necessary to break and form a multitude of specific contacts within nanoseconds after retinal isomerization in rhodopsin (or ligand binding in other GPCRs), but only a few near the central hinge region in order to induce allosteric changes in global conformation. While the case for the role of internal constraints release in the GPCR activation process is very strong, its precise mechanism has not been clear to date. The results described in this paper provide the first evidence for the *relaxation dynamics* of rhodopsin naturally favored by the interresidue contact topology in the dark state. They also confirm that only a few strong constraints exist, while the bulk of the molecule enjoys conformational mobility, as previously suggested.[53,70]

By definition, the motions predicted by the GNM/ANM are those along the smoothest ascent pathway away from the global minimum in a multidimensional free energy landscape. The proposed conformational changes are therefore the most favorable ones which the dark state will tend to undergo once a structural change has been triggered. Interestingly, these conformational changes provide an optimal 3D setting for (i) relieving the intermolecular steric clashes that would otherwise occur upon *cis* to *trans* isomerization of the retinal, and (ii) expose functional residues at the CP region, that can readily bind substrates such as the G protein.

We note that the GNM/ANM method relies upon the assumption that our structure is native-like and motions are similar to that native minimum in some coarse-grained energy landscape. It is clear that rhodopsin activation can be effected by changing the lipid environment; in our analysis we make no claims about how such changes to the lipid concentration or composition would impact our calculations. By not explicitly including the lipid in our model, we assume that its overall concentration/composition changes little during the conformational changes. On the other hand, rhodopsin activation has been pointed out to depend on the nature of the surrounding lipids. See for example, the work of Brown and collaborators[71] and the more recent work of Botelho et al.[72] Understanding the effect of lipid environment on the *intrinsic dynamics* of the protein would be a topic of utmost interest in future work. However, the present work focused on the identification of the intrinsic dynamics of rhodopsin, based on the premises that (i) the topology of interresidue contacts essentially determines the global motions of proteins, and (ii) the global modes are robust, that is, they are uniquely defined by the equilibrium structure and are insensitive to the details of atomic interactions, as elaborated

in several recent coarse-grained analyses of biomolecular equilibrium dynamics.[73] A recent analysis of the global dynamics of a series of potassium channels lend further support to the utility of examining the global dynamics of the proteins and identifying functional mechanisms (e.g., gate opening), regardless of the perturbations induced in the collective dynamics by the lipid environment.[74]

The predisposition of structures to undergo functional changes has been indicated in a number of recent studies.[30,32,38,40,75–77] A noteworthy example is the transition of hemoglobin from tense (T) to relaxed (R2–CO bound) form,[40] which was explained by the dominance of entropic effects (relaxation toward the least constrained state near the original state) in driving the functional reconfiguration of the molecule. The global torsion of rhodopsin that releases the constraints near the chromophore binding pocket and induces a weakening of intramolecular contacts at CP and EC regions also seems to be driven by entropic drives defined by the overall architecture. Notably, the most critical region controlling the collective changes in structure is located in the immediate neighborhood of the chromophore binding pocket, which is also the center of chemical activity/transition. Such a coupling between global mechanics and chemical activity demonstrated for a series of enzymes[31] appears to be a general design principle for proteins.

REFERENCES

1. Sakmar TP. Rhodopsin: a prototypical G protein-coupled receptor. Prog Nucleic Acid Res Mol Biol 1998;59:1–34.
2. Gether U. Uncovering molecular mechanisms involved in activation of G protein-coupled receptors. Endocr Rev 2000;21:90–113.
3. Muller G. Towards 3D structures of G protein-coupled receptors: a multidisciplinary approach. Curr Med Chem 2000;7:861–888.
4. Unger VM, Schertler GFX. Low-resolution structure of bovine rhodopsin determined by electron cryomicroscopy. Biophys J 1995;68:1776–1786.
5. Okada T, Palczewski K. Crystal structure of rhodopsin: implications for vision and beyond. Curr Opin Struct Biol 2001;11:420–426.
6. Okada T, Fujiyoshi Y, Silow M, Navarro J, Landau EM, Shichida Y. Functional role of internal water molecules in rhodopsin revealed by X-ray crystallography. Proc Natl Acad Sci USA 2002;99:5982–5987.
7. Okada T, Sugihara M, Bondar AN, Elstner M, Entel P, Buss V. The retinal conformation and its environment in rhodopsin in light of a new 2.2 A crystal structure. J Mol Biol 2004;342:571–583.
8. Palczewski K, Kumasaka T, Hori T, Behnke CA, Motoshima H, Fox BA, Le Trong I, Teller DC, Okada T, Stenkamp RE, Yamamoto M, Miyano M. Crystal structure of rhodopsin: a G protein-coupled receptor. Science 2000;289:739–745.
9. Teller DC, Okada T, Behnke CA, Palczewski K, Stenkamp RE. Advances in determination of a high-resolution three-dimensional structure of rhodopsin, a model of G-protein-coupled receptors (GPCRs). Biochemistry 2001;40:7761–7772.
10. Humphrey W, Dalke A, Schulten K. VMD: visual molecular dynamics. J Mol Graph 1996;14:33–38.
11. Hubbell WL, Altenbach C, Hubbell CM, Khorana HG. Rhodopsin structure, dynamics, and activation: a perspective from crystallography, site-directed spin labeling, sulfhydryl reactivity, and disulfide cross-linking. Adv Protein Chem 2003;63:243–290.
12. Klein-Seetharaman J. Dynamics in rhodopsin. Chembiochem 2002; 3:981–986.
13. Meng EC, Bourne HR. Receptor activation: what does the rhodopsin structure tell us? Trends Pharmacol Sci 2001;22:587–593.
14. Farrens DL, Khorana HG. Structure and function in rhodopsin. Measurement of the rate of metarhodopsin II decay by fluorescence spectroscopy. J Biol Chem 1995;270:5073–5076.
15. Rohrig UF, Guidoni L, Rothlisberger U. Early steps of the intramolecular signal transduction in rhodopsin explored by molecular dynamics simulations. Biochemistry 2002;41:10799–10809.
16. Saam J, Tajkhorshid E, Hayashi S, Schulten K. Molecular dynamics investigation of primary photoinduced events in the activation of rhodopsin. Biophys J 2002;83:3097–3112.
17. Crozier PS, Stevens MJ, Forrest LR, Woolf TB. Molecular dynamics simulation of dark-adapted rhodopsin in an explicit membrane bilayer: coupling between local retinal and larger scale conformational change. J Mol Biol 2003;333:493–514.
18. Huber T, Botelho AV, Beyer K, Brown MF. Membrane model for the G-protein-coupled receptor rhodopsin: hydrophobic interface and dynamical structure. Biophys J 2004;86:2078–2100.
19. Lemaitre V, Yeagle P, Watts A. Molecular dynamics simulations of retinal in rhodopsin: from the dark-adapted state towards lumirhodopsin. Biochemistry 2005;44:12667–12680.
20. Ishiguro M, Hirano T, Oyama Y. Modelling of photointermediates suggests a mechanism of the flip of the β-ionone moiety of the retinylidene chromophore in the rhodopsin photocascade. Chembiochem 2003;4:228–231.
21. Ishiguro M, Oyama Y, Hirano T. Structural models of the photointermediates in the rhodopsin photocascade, lumirhodopsin, metarhodopsin I, and metarhodopsin II. Chembiochem 2004;5: 298–310.
22. Choi G, Landin J, Galan JF, Birge RR, Albert AD, Yeagle PL. Structural studies of metarhodopsin II, the activated form of the G-protein coupled receptor, rhodopsin. Biochemistry 2002;41: 7318–7324.
23. Gouldson PR, Kidley NJ, Bywater RP, Psaroudakis G, Brooks HD, Diaz C, Shire D, Reynolds CA. Toward the active conformations of rhodopsin and the β2-adrenergic receptor. Proteins 2004;56:67–84.
24. Nikiforovich GV, Marshall GR. Three-dimensional model for Meta-II rhodopsin, an activated G-protein-coupled receptor. Biochemistry 2003;42:9110–9120.
25. Nikiforovich GV, Marshall GR. Modeling flexible loops in the dark-adapted and activated states of rhodopsin, a prototypical G-protein-coupled receptor. Biophys J 2005;89:3780–3789.
26. Bahar I, Atilgan AR, Erman B. Direct evaluation of thermal fluctuations in proteins using a single-parameter harmonic potential. Fold Des 1997;2:173–181.
27. Haliloglu T, Bahar I, Erman B. Gaussian dynamics of folded proteins. Phys Rev Lett 1997;79:3090–3093.
28. Flory PJ. Statistical thermodynamics of random networks. Proc R Soc Lond A 1976;351:351–380.
29. Atilgan AR, Durell SR, Jernigan RL, Demirel MC, Keskin O, Bahar I. Anisotropy of fluctuation dynamics of proteins with an elastic network model. Biophys J 2001;80:505–515.
30. Bahar I, Rader AJ. Coarse-grained normal mode analysis in structural biology. Curr Opin Struct Biol 2005;15:586–592.
31. Yang LW, Bahar I. Coupling between catalytic site and collective dynamics: a requirement for mechanochemical activity of enzymes. Structure 2005;13:893–904.
32. Tama F, Sanejouand YH. Conformational change of proteins arising from normal mode calculations. Protein Eng 2001;14:1–6.
33. Tama F, Wriggers W, Brooks CL. Exploring global distortions of biological macromolecules and assemblies from low-resolution structural information and elastic network theory. J Mol Biol 2002;321:297–305.
34. Rader AJ, Anderson G, Isin B, Khorana HG, Bahar I, Klein-Seetharaman J. Identification of core amino acids stabilizing rhodopsin. Proc Natl Acad Sci USA 2004;101:7246–7251.
35. Ming D, Kong YF, Lambert MA, Huang Z, Ma JP. How to describe protein motion without amino acid sequence and atomic coordinates. Proc Natl Acad Sci USA 2002;99:8620–8625.
36. Isin B, Doruker P, Bahar I. Functional motions of influenza virus hemagglutinin: a structure-based analytical approach. Biophys J 2002;82:569–581.
37. Chennubhotla C, Rader AJ, Yang LW, Bahar I. Elastic network models for understanding biomolecular machinery: from enzymes to supramolecular assemblies. Phys Biol 2005;2:S173–S180.
38. Ma J. Usefulness and limitations of normal mode analysis in modeling dynamics of biomolecular complexes. Structure 2005;13: 373–380.
39. Berman HM, Westbrook J, Feng Z, Gilliland G, Bhat TN, Weissig H, Shindyalov IN, Bourne PE. The protein data bank. Nucleic Acids Res 2000;28:235–242.

40. Xu C, Tobi D, Bahar I. Allosteric changes in protein structure computed by a simple mechanical model: hemoglobin T<-> R2 transition. J Mol Biol 2003;333:153–168.
41. Cornell WD, Cieplak P, Bayly CI, Gould IR, Merz KM, Ferguson DM, Spellmeyer DC, Fox T, Caldwell JW, Kollman PA. A second generation force field for the simulation of proteins, nucleic acids, and organic molecules. J Am Chem Soc 1995;117:5179–5197.
42. Alewijnse AE, Timmerman H, Jacobs EH, Smit MJ, Roovers E, Cotecchia S, Leurs R. The effect of mutations in the DRY motif on the constitutive activity and structural instability of the histamine H(2) receptor. Mol Pharmacol 2000;57:890–898.
43. Ballesteros J, Kitanovic S, Guarnieri F, Davies P, Fromme BJ, Konvicka K, Chi L, Millar RP, Davidson JS, Weinstein H, Sealfon SC. Functional microdomains in G-protein-coupled receptors. The conserved arginine-cage motif in the gonadotropin-releasing hormone receptor. J Biol Chem 1998;273:10445–10453.
44. Ballesteros JA, Jensen AD, Liapakis G, Rasmussen SG, Shi L, Gether U, Javitch JA. Activation of the β2-adrenergic receptor involves disruption of an ionic lock between the cytoplasmic ends of transmembrane segments 3 and 6. J Biol Chem 2001;276:29171–29177.
45. Baranski TJ, Herzmark P, Lichtarge O, Gerber BO, Trueheart J, Meng EC, Iiri T, Sheikh SP, Bourne HR. C5a receptor activation. Genetic identification of critical residues in four transmembrane helices. J Biol Chem 1999;274:15757–15765.
46. Cohen GB, Yang T, Robinson PR, Oprian DD. Constitutive activation of opsin: influence of charge at position 134 and size at position 296. Biochemistry 1993;32:6111–6115.
47. Greasley PJ, Fanelli F, Rossier O, Abuin L, Cotecchia S. Mutagenesis and modelling of the α1b-adrenergic receptor highlight the role of the helix 3/helix 6 interface in receptor activation. Mol Pharmacol 2002;61:1025–1032.
48. Hogger P, Shockley MS, Lameh J, Sadee W. Activating and inactivating mutations in N- and C-terminal i3 loop junctions of muscarinic acetylcholine Hm1 receptors. J Biol Chem 1995;270: 7405–7410.
49. Rasmussen SG, Jensen AD, Liapakis G, Ghanouni P, Javitch JA, Gether U. Mutation of a highly conserved aspartic acid in the β2 adrenergic receptor: constitutive activation, structural instability, and conformational rearrangement of transmembrane segment 6. Mol Pharmacol 1999;56:175–184.
50. Samama P, Cotecchia S, Costa T, Lefkowitz RJ. A mutation-induced activated state of the β2-adrenergic receptor. Extending the ternary complex model. J Biol Chem 1993;268:4625–4636.
51. Scheer A, Fanelli F, Costa T, De Benedetti PG, Cotecchia S. Constitutively active mutants of the α_{1b}-adrenergic receptor: role of highly conserved polar amino acids in receptor activation. Embo J 1996;15:3566–3478.
52. Shi L, Liapakis G, Xu R, Guarnieri F, Ballesteros JA, Javitch JA. β2 adrenergic receptor activation. Modulation of the proline kink in transmembrane 6 by a rotamer toggle switch. J Biol Chem 2002;277:40989–40996.
53. Klein-Seetharaman J, Yanamala NV, Javeed F, Reeves PJ, Getmanova EV, Loewen MC, Schwalbe H, Khorana HG. Differential dynamics in the G protein-coupled receptor rhodopsin revealed by solution NMR. Proc Natl Acad Sci USA 2004;101:3409–3413.
54. Borhan B, Souto ML, Imai H, Shichida Y, Nakanishi K. Movement of retinal along the visual transduction path. Science 2000;288: 2209–2212.
55. Nakayama TA, Khorana HG. Orientation of retinal in bovine rhodopsin determined by cross-linking using a photoactivatable analog of 11-*cis*-retinal. J Biol Chem 1990;265:15762–15769.
56. Nakayama TA, Khorana HG. Mapping of the amino acids in membrane-embedded helices that interact with the retinal chromophore in bovine rhodopsin. J Biol Chem 1991;266:4269–4275.
57. Ridge KD, Bhattacharya S, Nakayama TA, Khorana HG. Light-stable rhodopsin. II. An opsin mutant (TRP-265----Phe) and a retinal analog with a nonisomerizable 11-*cis* configuration form a photostable chromophore. J Biol Chem 1992;267:6770–6775.
58. Visiers I, Ballesteros JA, Weinstein H. Three-dimensional representations of G protein-coupled receptor structures and mechanisms. Methods Enzymol 2002;343:329–371.
59. Sakmar TP, Franke RR, Khorana HG. The role of the retinylidene Schiff base counterion in rhodopsin in determining wavelength absorbance and Schiff base pKa. Proc Natl Acad Sci USA 1991;88: 3079–3083.
60. Altenbach C, Yang K, Farrens DL, Farahbakhsh ZT, Khorana HG, Hubbell WL. Structural features and light-dependent changes in the cytoplasmic interhelical E-F loop region of rhodopsin: a site-directed spin-labeling study. Biochemistry 1996; 35:12470–12478.
61. Altenbach C, Klein-Seetharaman J, Hwa J, Khorana HG, Hubbell WL. Structural features and light-dependent changes in the sequence 59–75 connecting helices I and II in rhodopsin: a site-directed spin-labeling study. Biochemistry 1999;38:7945–7949.
62. Altenbach C, Cai K, Khorana HG, Hubbell WL. Structural features and light-dependent changes in the sequence 306–322 extending from helix VII to the palmitoylation sites in rhodopsin: a site-directed spin-labeling study. Biochemistry 1999;38:7931–7937.
63. Cai K, Langen R, Hubbell WL, Khorana HG. Structure and function in rhodopsin: topology of the C-terminal polypeptide chain in relation to the cytoplasmic loops. Proc Natl Acad Sci USA 1997;94:14267–14272.
64. Farahbakhsh ZT, Ridge KD, Khorana HG, Hubbell WL. Mapping light-dependent structural changes in the cytoplasmic loop connecting helices C and D in rhodopsin: a site-directed spin labeling study. Biochemistry 1995;34:8812–8819.
65. Farrens DL, Altenbach C, Yang K, Hubbell WL, Khorana HG. Requirement of rigid-body motion of transmembrane helices for light activation of rhodopsin. Science 1996;274:768–770.
66. Klein-Seetharaman J, Hwa J, Cai K, Altenbach C, Hubbell WL, Khorana HG. Probing the dark state tertiary structure in the cytoplasmic domain of rhodopsin: proximities between amino acids deduced from spontaneous disulfide bond formation between Cys316 and engineered cysteines in cytoplasmic loop 1. Biochemistry 2001;40:12472–12478.
67. Cai K, Klein-Seetharaman J, Hwa J, Hubbell WL, Khorana HG. Structure and function in rhodopsin: effects of disulfide cross-links in the cytoplasmic face of rhodopsin on transducin activation and phosphorylation by rhodopsin kinase. Biochemistry 1999;38: 12893–12898.
68. Klco JM, Wiegand CB, Narzinski K, Baranski TJ. Essential role for the second extracellular loop in C5a receptor activation. Nat Struct Mol Biol 2005;12:320–326.
69. Massotte D, Kieffer BL. The second extracellular loop: a damper for G protein-coupled receptors? Nat Struct Mol Biol 2005;12: 287–288.
70. Klein-Seetharaman J, Reeves PJ, Loewen MC, Getmanova EV, Chung J, Schwalbe H, Wright PE, Khorana HG. Solution NMR spectroscopy of [α-15N]lysine-labeled rhodopsin: the single peak observed in both conventional and TROSY-type HSQC spectra is ascribed to Lys-339 in the carboxyl-terminal peptide sequence. Proc Natl Acad Sci USA 2002;99:3452–3457.
71. Brown MF. Modulation of rhodopsin function by properties of the membrane bilayer. Chem Phys Lipids 1994;73:159–180.
72. Botelho AV, Gibson NJ, Thurmond RL, Wang Y, Brown MF. Conformational energetics of rhodopsin modulated by nonlamellar-forming lipids. Biochemistry 2002;41:6354–6368.
73. Cui Q, Bahar I. Normal mode analysis theory and applications in biological and chemical systems. Boca Raton, FL: Taylor & Francis Group; 2006. p. 406.
74. Shrivastava IH, Bahar I. Common mechanism of pore opening shared by five different potassium channels. Biophys J 2006;90: 3929–3940.
75. Changeux JP, Edelstein SJ. Allosteric mechanisms of signal transduction. Science 2005;308:1424–1428.
76. Eisenmesser EZ, Millet O, Labeikovsky W, Korzhnev DM, Wolf-Watz M, Bosco DA, Skalicky JJ, Kay LE, Kern D. Intrinsic dynamics of an enzyme underlies catalysis. Nature 2005;438:117–121.
77. Tobi D, Bahar I. Structural changes involved in protein binding correlate with intrinsic motions of proteins in the unbound state. Proc Natl Acad Sci USA 2005;102:18908–18913.